Journal of Power Sources 196 (2011) 4972–4979

Contents lists available at ScienceDirect

Journal of Power Sources

journal homepage: www.elsevier.com/locate/jpowsour

Oxygen reduction reaction via the 4-electron transfer pathway on transition metal hydroxides

Zi Xuan Liu [a], Zhou Peng Li [a,*], Hai Ying Qin [a], Bin Hong Liu [b]

[a] Department of Chemical and Biological Engineering, Zhejiang University, Zeda Road 38, Hangzhou, Zhejiang 310027, PR China
[b] Department of Materials Science and Engineering, Zhejiang University, Hangzhou 310027, PR China

ARTICLE INFO

Article history:
Received 29 November 2010
Received in revised form 11 January 2011
Accepted 31 January 2011
Available online 2 March 2011

Keywords:
Oxygen reduction reaction
Hydroxide
Oxyhydroxide
Electrocatalytic activity
Redox couple

ABSTRACT

Carbon-supported $Co(OH)_2$ and $Ni(OH)_2$ catalysts are prepared to examine the mechanism of oxygen reduction reaction (ORR) on hydroxide catalysts. ORR via the 4-electron transfer pathway on a hydroxide undergoes oxidation of hydroxide by O_2 to form oxyhydroxide, followed by electrochemical reaction of oxyhydroxide to regain hydroxide. β-$Ni(OH)_2$ has the same crystal structure and lattice parameters as β-$Co(OH)_2$, but it exhibits a poorer catalytic activity toward ORR than β-$Co(OH)_2$ at a low temperature. The poor catalytic activity of $Ni(OH)_2$/C can be attributed to the difficulty in $Ni(OH)_2$ oxidation and the slow kinetics of NiOOH electroreduction to $Ni(OH)_2$. The catalytic activity of the $Ni(OH)_2$/C catalyst is significantly improved through elevating the operation temperature because $Ni(OH)_2$ oxidation to NiOOH and NiOOH electroreduction are improved at a high temperature. A model of ORR via the 4-electron transfer pathway on transition metal hydroxides is suggested and discussed.

© 2011 Elsevier B.V. All rights reserved.

1. Introduction

Fuel cells are energy conversion instruments by which the chemical energy in various fuels is converted to electricity with high efficiency. During cell operation, fuel is oxidized at the anode side, and oxygen is reduced at the cathode side. The cell performance is highly dependent on cathode polarization related to the oxygen reduction reaction (ORR) on the cathode catalyst.

Pt exists in metallic form during fuel cell operation. It is the best cathode catalyst for ORR due to its excellent electrocatalytic activity and electrical conductivity. However, the scarcity of Pt in resources is a major problem in the application of fuel cells, especially those operating at a low temperature. Therefore, the development of alternative catalysts is one of the critical issues in fuel cell technologies [1,2].

Cyclic organic compounds [2]; non-platinum metals such as Cu [3], Ni [4], Ag [5,6], Co [7–10], or bimetallic catalysts [11]; and cobalt compounds such as $LaCoO_3$ [12], cobalt hydroxide [13,14] and nitrides [15] have been used as catalysts for ORR. Beck [16] found that transition metal cations with a low chemical valence in metallophthalocyanines are oxidized when O_2 is adsorbed on cations M(II), and then molecular O_2 is partially reduced to the superoxide state during ORR as shown in the following:

$$M(II) + O_2 = [M(III)–O_2]^- \quad (1)$$

$$[M(III)–O_2]^- + e^- \rightarrow M(II) + \text{intermediates} \quad (2)$$

The potential of the M(III)/M(II) redox couple is an important parameter in determining electrocatalytic activity toward ORR on metallophthalocyanine catalysts [17]. The more positive the potential of the M(III)/M(II) redox couple, the higher the electrocatalytic activity of the catalyst [18]. Wass et al. [19] studied the ORR mechanism on $Co(OH)_2$, suggesting a redox cycle via a 2-electron transfer pathway of oxygen electroreduction to hydrogen peroxide on $Co(OH)_2$. However, the mechanism of ORR on hydroxides via a 4-electron transfer pathway has not been elucidated.

To examine the effect of oxyhydroxide formation on the electrocatalytic activity of hydroxides toward ORR, cobalt hydroxide and nickel hydroxide are selected as target samples. Cobalt and nickel hydroxides have similar general chemical properties but exhibit distinct redox potentials as follows:

$$Co(OH)_2 + OH^- = CoOOH + H_2O + e^- \quad E^\circ = 0.17\,\text{Vvs.SHE} \quad (3)$$

$$Ni(OH)_2 + OH^- = NiOOH + H_2O + e^- \quad E^\circ = 0.52\,\text{Vvs.SHE} \quad (4)$$

Based on material characterizations and electrochemical evaluations, the ORR mechanism on transition hydroxide catalysts is suggested and discussed in this work.

* Corresponding author. Tel.: +86 571 87953149; fax: +86 571 87953149.
E-mail address: zhoupengli@zju.edu.cn (Z.P. Li).

0378-7753/$ – see front matter © 2011 Elsevier B.V. All rights reserved.
doi:10.1016/j.jpowsour.2011.01.102

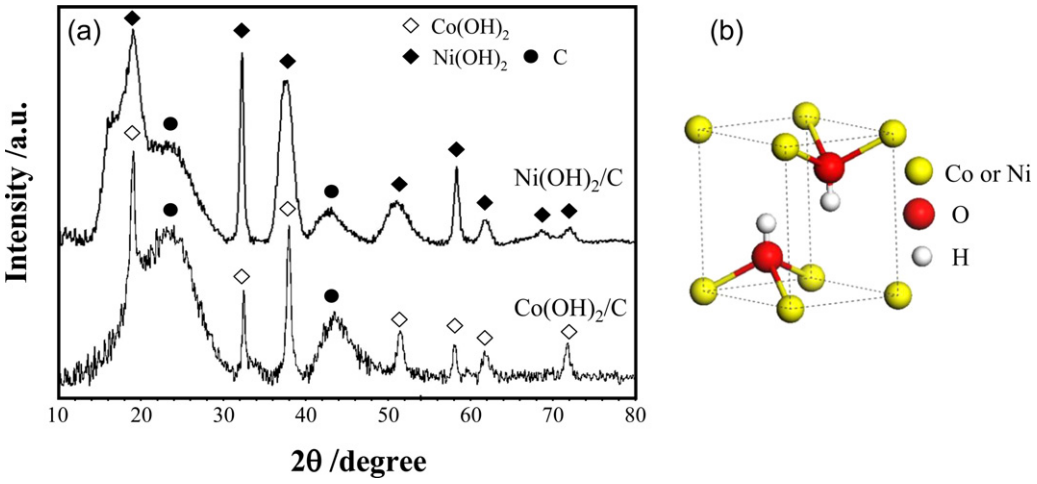

Fig. 1. (a) XRD patterns of synthesized $Co(OH)_2$/C and $Ni(OH)_2$/C catalysts, and (b) corresponding schematic structure of the hydroxides.

2. Experimental details

The carbon-supported $Co(OH)_2$ ($Co(OH)_2$/C) and $Ni(OH)_2$ ($Ni(OH)_2$/C) catalysts were prepared by chemical deposition method. To a carbon dispersion solution (60 mL) containing 2.7 g of activated carbon (BP2000 from Cabot Corp.), 15 mL of $NiCl_2$ or $CoCl_2$ solution (0.36 mol L^{-1}) was added. After stirring the above mixture at 80 °C for 30 min, 300 mL of the NaOH solution (0.03 mol L^{-1}) was added at a rate of 20 mL min^{-1} with a peristaltic pump. The applied catalysts were then obtained by drying at 90 °C for 12 h under a vacuum after filtering and washing with warm de-ionized water. The content of $Ni(OH)_2$ or $Co(OH)_2$ in the carbon supported catalyst was measured to be 15 wt.%.

The catalyst structure was identified by X-ray diffraction (XRD) with a Rigaku D/MAX-2550-PC X-ray diffractometer using Cu Kα radiation (λ = 1.54059 Å, operated at 40 kV, 250 mA). Catalyst morphology was observed with a JEM-2010 transmission electron microscope (TEM). The chemical valence states of Ni or Co in the catalyst surface layer were identified by X-ray photoemission spectroscopy (XPS) (Kratos AXIS Ultra DLD).Cyclic voltammetry tests were conducted with a Zahner IM6 electrochemical workstation using a BASi RDE2 rotating disk electrode (RDE, 3 mm in diameter). A piece of Pt wire was used as the counter electrode, and an Hg/6 M KOH/HgO electrode was used as the reference electrode connecting to the cell with a salt bridge. The potential of the Hg/HgO/1 M KOH electrode is +0.098 V vs. the reversible hydrogen electrode (RHE) in basic solution. The potentials vs. RHE can be calculated using the following relation:

$$E(\text{Vvs.RHE}) = E(\text{Vvs.Hg/HgO/6 MKOH}) + 0.037 + 0.0591 \times \text{pHat25 °C} \quad (5)$$

where 0.037 is the potential of Hg/HgO/6 M KOH electrode vs. SHE at 25 °C, and 0.0591 is obtained from $2.303RT/nF$ according to the Hg/HgO/6 M KOH reference electrode. pH value is measured by a pH meter. All potential values are expressed in potential vs. Hg/HgO/6 M KOH reference electrode. The working electrode was prepared as follows. Ten milligrams of the catalyst was ultrasonically mixed with 0.1 mL of Nafion solution (5 wt.%) and 1.5 mL of ethanol to form a homogeneous ink. Then the ink was pipetted onto the pretreated glassy carbon (GC) electrode and dried at room temperature. All CV curves were measured in 1 M NaOH solution.

A single cell with an active area of 6 cm^2 was assembled to evaluate cathode polarization. The cell configuration was the same as described in our previous paper [20]. The cathode was prepared by coating a catalyst slurry containing a catalyst, Nafion solution (5 wt.%), ethanol, and de-ionized water with a mass ratio of 1:7:3:3 onto a piece of hydrophobic carbon cloth. The anode preparation and Nafion 117 membrane pretreatment have been described elsewhere [9]. An alkaline $NaBH_4$ solution containing $NaBH_4$ (5 wt.%) and NaOH (10 wt.%) was used as fuel (anolyte). Polarization behavior was evaluated using a PFX-2011 battery tester (Kikusui Electronics Corp.) at a fuel flow rate of 38 mL min^{-1} and humidified O_2 flow rate of 1.5 L min^{-1} at 20 or 60 °C under 1 atm. An Hg/HgO/6 M KOH electrode was used as the reference electrode connecting to the anolyte (alkaline $NaBH_4$ solution) with a salt bridge.

3. Results and discussion

3.1. Catalyst characterizations

Fig. 1 shows the XRD patterns of the as-prepared $Co(OH)_2$/C and $Ni(OH)_2$/C catalysts, indicating that the $Co(OH)_2$/C catalyst consists of carbon and β-$Co(OH)_2$, and the $Ni(OH)_2$/C catalyst consists of carbon and β-$Ni(OH)_2$. β-$Co(OH)_2$ and β-$Ni(OH)_2$ have the same hexagonal closest-packed (HCP) structure with the same lattice parameters as illustrated in Fig. 1(b). The nano ribbons of β-$Ni(OH)_2$ and β-$Co(OH)_2$ are similar in size and shape as shown in the TEM observations in Fig. 2. Their high-resolution transmission electron microscopy (HRTEM) images indicate that both β-$Ni(OH)_2$ and β-$Co(OH)_2$ have the same (0 0 1) interplanar spacing of 0.46 nm, which agrees well with the XRD results.

Fig. 3 shows the cathode polarization in a direct borohydride fuel cell (DBFC) using $Ni(OH)_2$/C or $Co(OH)_2$/C as the cathode catalyst under an operation current density of 40 mA cm^{-2} at 20 °C. DBFCs use alkaline borohydride solutions as fuel [20]. Unlike the $Co(OH)_2$/C cathode, the $Ni(OH)_2$/C cathode exhibits an unstable polarization behavior. The XRD patterns of the $Co(OH)_2$/C and $Ni(OH)_2$/C catalysts after use are illustrated in Fig. 4. For the $Co(OH)_2$/C catalyst, the fingerprint diffraction peak of β-$Co(OH)_2$ at 32.4° in 2θ (corresponding to (1 0 0) planes) disappears after use. The XRD pattern matches the JCPDS (72-2280) file, identifying the existence of β-CoOOH. However, only a small XRD peak identified as β-NiOOH in Fig. 4(b) appears for the $Ni(OH)_2$/C catalyst after use, indicating that only a small portion of nickel hydroxide has been converted to nickel oxyhydroxide. Fig. 5 shows the HRTEM images of the $Co(OH)_2$/C and $Ni(OH)_2$/C catalysts after use at 20 °C. The interplanar spacing of 0.42 nm [in Fig. 5(a)] refers to the existence of β-CoOOH in the $Co(OH)_2$/C catalyst. The interplanar spacing of 0.48 nm [in Fig. 5(b)] refers to the existence of

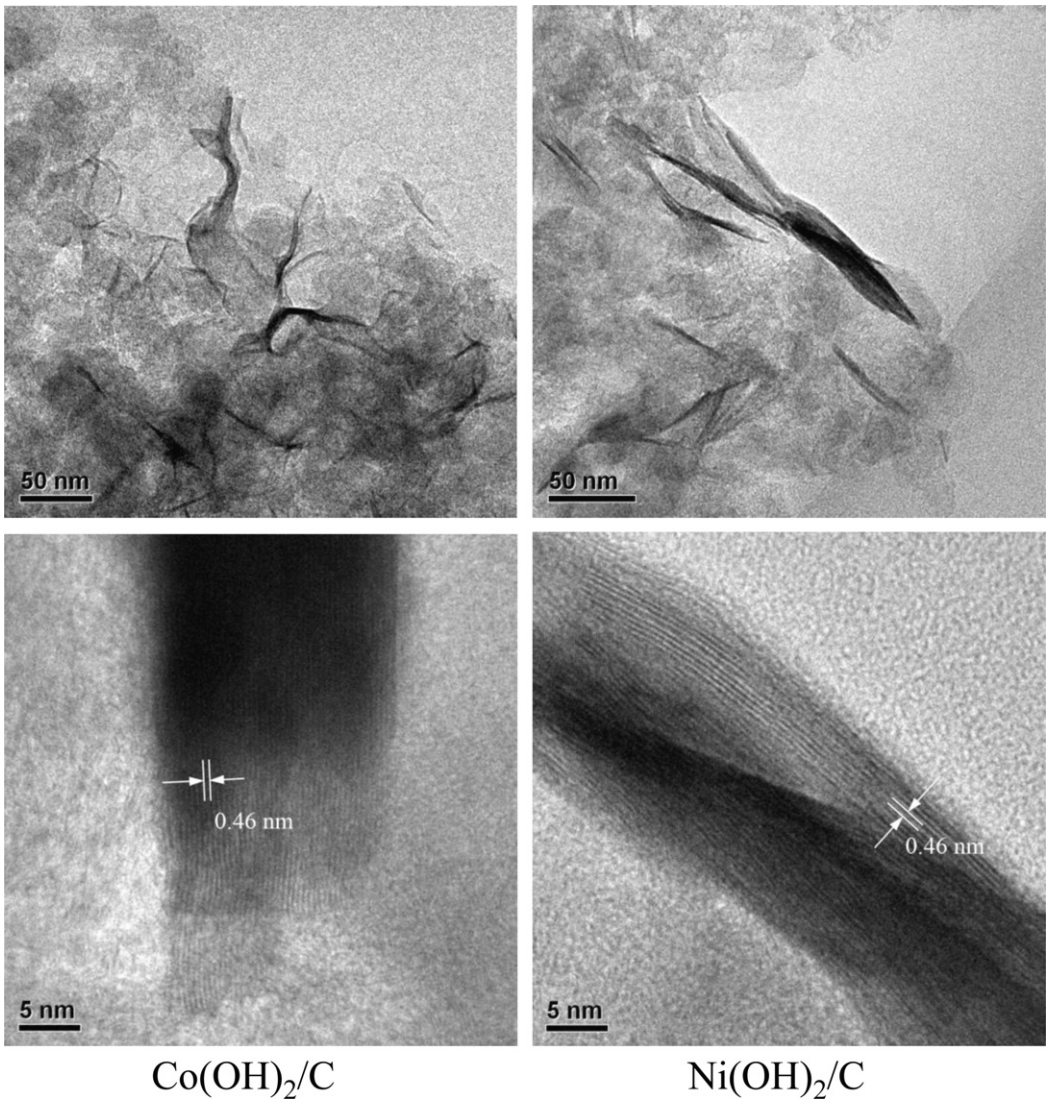

Fig. 2. TEM images of the as-prepared $Co(OH)_2$/C and $Ni(OH)_2$/C catalysts.

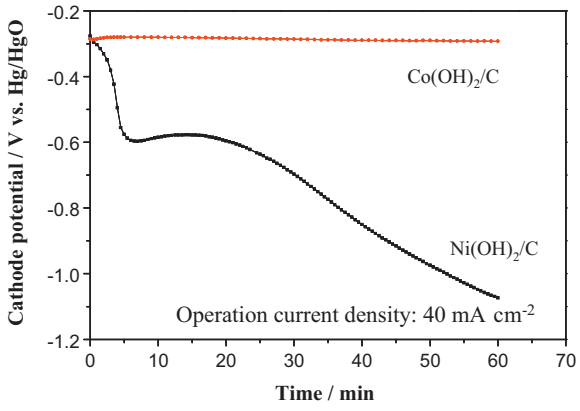

Fig. 3. Polarization behavior of the cathode using $Co(OH)_2$/C or $Ni(OH)_2$/C as the catalyst in the DBFC at 20 °C. Anode: Zr–Ni alloy/Ni/Pd/C, catalyst loading: 10 mg cm^{-2}. Anolyte: 5 wt.% of $NaBH_4$, 10 wt.% of NaOH, pH 14.19. Cathode: catalyst loading: 5 mg cm^{-2}, humidified O_2 at a flow rate of 1.5 L min^{-1}. Both anode and cathode area: 6 cm^2. Reference electrode: Hg/HgO/6 M KOH.

β-NiOOH in the β-$Ni(OH)_2$ crystal of the $Ni(OH)_2$/C catalyst after use. Therefore, most of β-$Co(OH)_2$ is converted to β-CoOOH in the $Co(OH)_2$/C catalyst, but only a small amount of β-$Ni(OH)_2$ is converted to β-NiOOH in the $Ni(OH)_2$/C catalyst during ORR occurrence at 20 °C.

3.2. Electrochemical evaluations

To understand the relationship of electrocatalytic activity and oxyhydroxide formation during ORR, cyclic voltammetry (CV) measurements of the $Ni(OH)_2$/C and $Co(OH)_2$/C electrodes were carried out in NaOH solution saturated with Ar or O_2. Before each CV measurement, cyclic potential sweeps between −0.3 and 0 V in Ar-saturated NaOH solution were conducted to ensure that the test catalysts exist in hydroxide form rather than in oxyhydroxide form.

3.2.1. ORR on $Co(OH)_2$/C

Fig. 6(a) shows the CVs using the $Co(OH)_2$/C-GC electrodes with different $Co(OH)_2$ contents in the Ar-saturated NaOH solution (1 M). The cathodic current peak area at −0.1 V increases with an increase in $Co(OH)_2$ content in the electrode. As pointed out by Pralong [21], CoOOH can be obtained through the electrooxidation

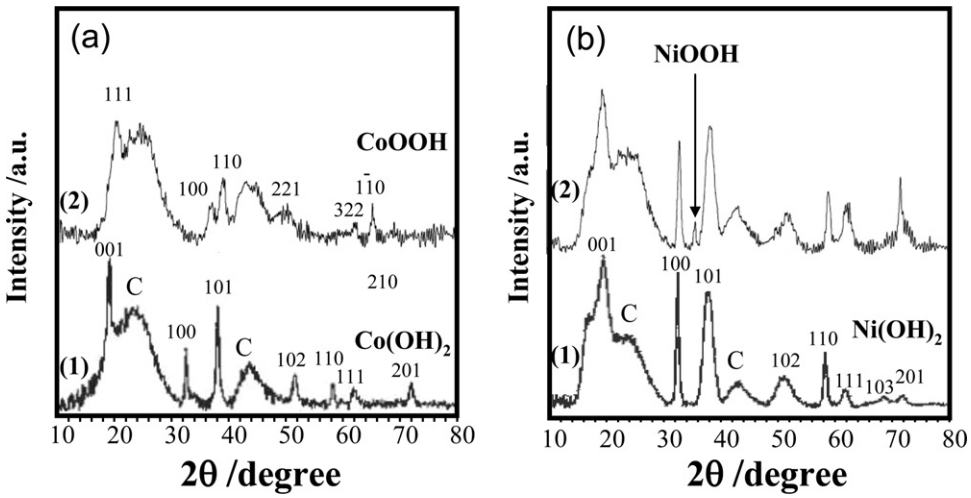

Fig. 4. XRD patterns of (a) $Co(OH)_2$/C and (b) $Ni(OH)_2$/C (1) before and (2) after use.

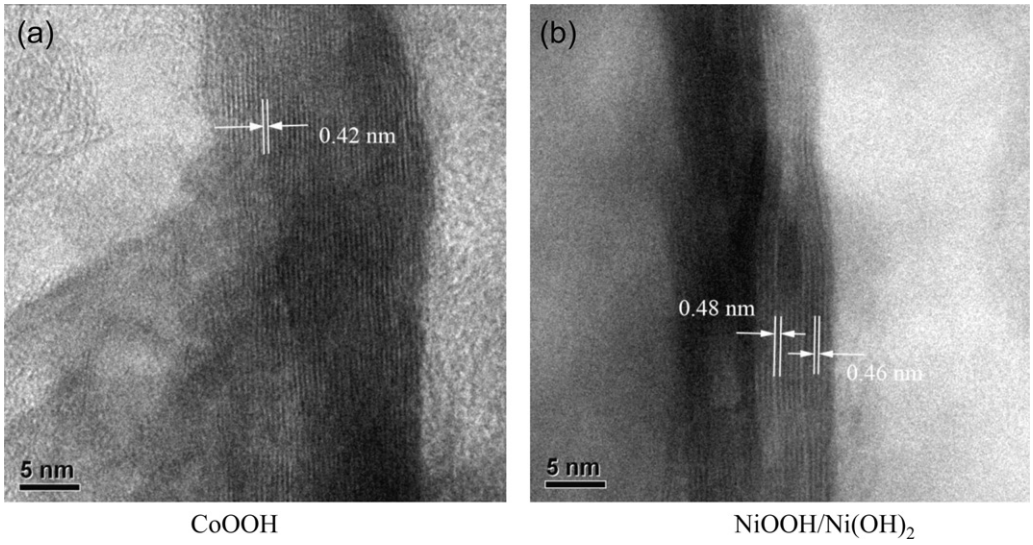

Fig. 5. HRTEM images of the $Co(OH)_2$/C and $Ni(OH)_2$/C catalysts after use at 20 °C.

reaction of $Co(OH)_2$. Therefore, the cathodic current at −0.1 V vs. Hg/HgO is caused by the electroreduction of CoOOH formed during the anodic process of CV based on reaction (3).

The cyclic voltammograms of the $Co(OH)_2$/C modified glassy-carbon electrode in the NaOH solutions saturated with Ar or O_2 were measured with different switching potentials (from 0.2 to 0.4 V), as shown in Fig. 7(a). The cathodic peak area (at −0.1 V) measured in the O_2-saturated NaOH solution was obviously larger than that measured in the Ar-saturated NaOH solution. The linear sweep voltammograms of the $Co(OH)_2$/C electrode in the NaOH solution bubbled with O_2 for different time periods were recorded as shown in Fig. 8(a). The cathodic peak current increased with an increase in O_2 bubbling time. These results indicated that ORR occurs at the same potential as CoOOH electroreduction.

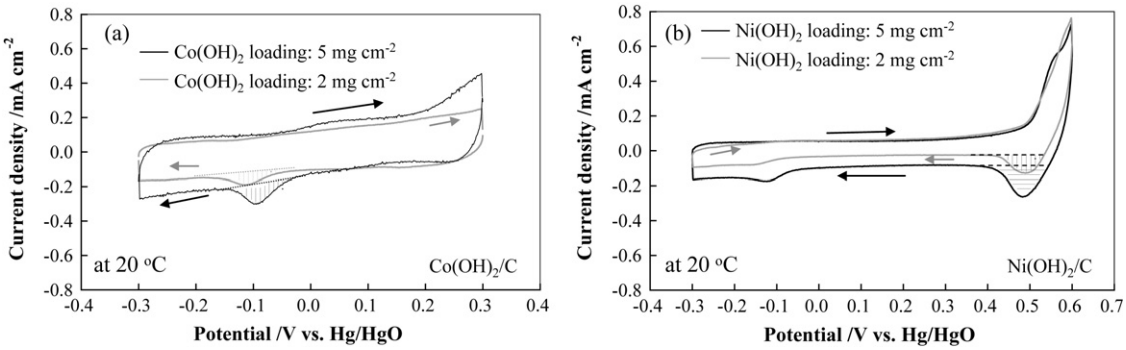

Fig. 6. Cyclic voltammograms of (a) $Co(OH)_2$/C and (b) $Ni(OH)_2$/C modified glassy-carbon electrodes with different hydroxide contents at a scan rate of 10 mV s^{-1} in Ar-saturated NaOH solution (1 M, pH 13.78) at 20 °C. Electrode area: 0.07 cm^2. Reference electrode: Hg/HgO/6 M KOH.

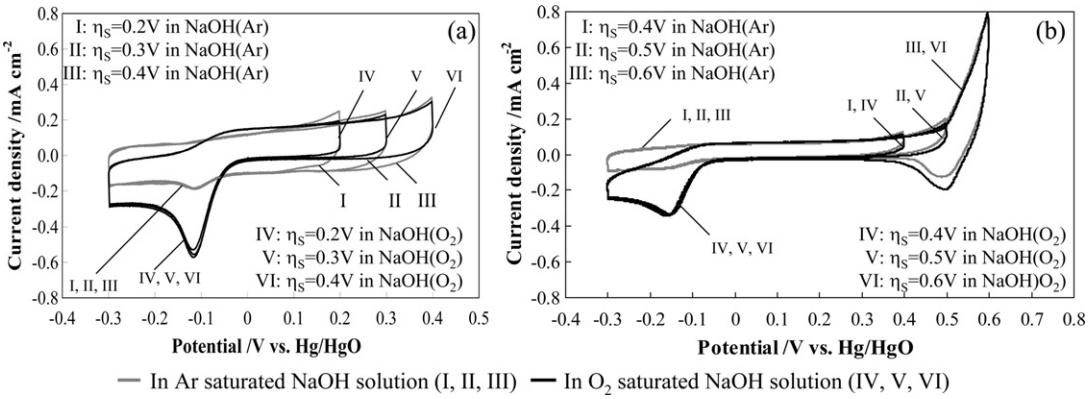

Fig. 7. Cyclic voltammograms of (a) $Co(OH)_2$/C and (b) $Ni(OH)_2$/C modified glassy-carbon electrode at a scan rate of 10 mV s^{-1} in Ar or O_2 saturated NaOH solutions [1 M NaOH(Ar) or NaOH(O_2), pH 13.78], with different switching potentials (η_S) at 20 °C. Catalyst loading: 2 mg cm^{-2}. Electrode area: 0.07 cm^2. Reference electrode: Hg/HgO/6 M KOH.

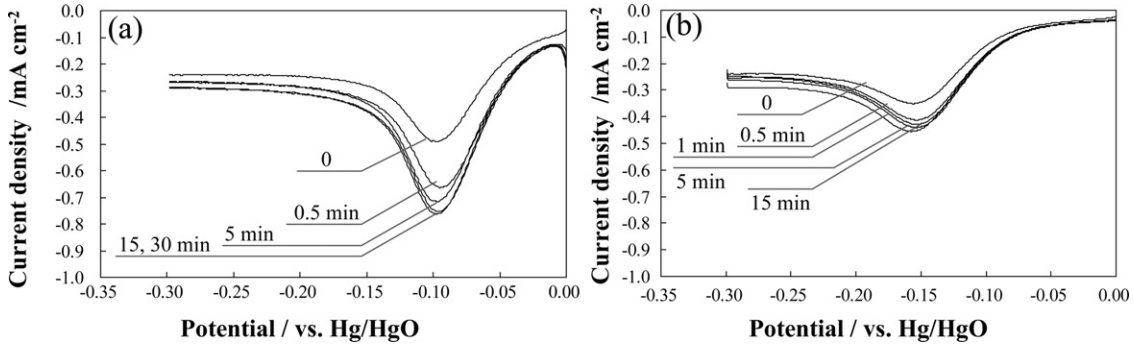

Fig. 8. Cathodic potential–current relationship of (a) $Co(OH)_2$/C and (b) $Ni(OH)_2$ modified glassy-carbon electrodes in NaOH solution (1 M, pH 13.78) bubbled with O_2 for different time periods at 20 °C. Scan rate: 10 mV s^{-1}. Catalyst loading: 5 mg cm^{-2}. Electrode area: 0.07 cm^2. Reference electrode: Hg/HgO/6 M KOH.

There was a certain increase in anodic current in the anodic process of CV measurements in the NaOH solution saturated with O_2 rather than Ar. This implied that something was formed during ORR in the cathodic process of CV measurement, and the formed substance was then oxidized in the following anodic process. The 2-electron reduction reaction of oxygen on $Co(OH)_2$/C possibly generated H_2O_2 according to Wass et al.'s findings [19]. The anodic current appearing around 0 V might be caused by H_2O_2 oxidation. The linear sweep voltammograms of the $Co(OH)_2$/C modified glassy-carbon electrode in the NaOH solutions containing different amounts of H_2O_2 were recorded as shown in Fig. 9. The anodic behavior of the $Co(OH)_2$/C electrode in the Ar-saturated NaOH solutions containing H_2O_2 was similar to that of the $Co(OH)_2$/C electrode in the O_2-saturated NaOH solution as shown in Fig. 7(a). The anodic current increased with an increase in H_2O_2 content in the Ar saturated NaOH solutions. Therefore, the ORR on $Co(OH)_2$ is assumed to be an incomplete 4-electron-reaction, and H_2O_2 is formed during ORR.

To evaluate the number of electrons for ORR on $Co(OH)_2$, voltammetry measurements using rotating disk electrode (RDE) were performed. The number (n) of transferred electrons for ORR on the applied catalysts can be determined through the Koutecky–Levich (K–L) plots as follows [22]:

$$j^{-1} = jk^{-1} + \{0.62nFC_{O_2}D_{O_2}^{2/3}\nu^{-1/6}\omega^{1/2}\}^{-1} \quad (6)$$

where j is the measured current density, j_k is the kinetic current density, n is the number of electrons transferred per O_2 molecule, and F is the Faraday constant. The values of the concentration of O_2 (C_{O_2}), the diffusion coefficient (D_{O_2}) of O_2 in 0.1 M KOH solution, and the kinematic viscosity (ν) of 0.1 M KOH solution are 1.15×10^{-3} M, 1.95×10^{-5} cm^2 s^{-1}, and 0.008977 cm^2 s^{-1}, respectively [22]. ω stands for the rotation rate (rad s^{-1}). K–L plots are obtained from the RDE voltammograms in 0.1 M KOH solution using the limiting currents at 0.3, 0.4, and 0.5 V as shown in the inset of Fig. 10(a) because no data can be cited in the NaOH solutions.

From the slopes of the K–L plots, the values of n for ORR on the $Co(OH)_2$/C electrode are calculated as 2.86, 2.94, and 3.00 at 0.3, 0.4, and 0.5 V, respectively. The number of electrons exchanged in the O_2 reduction reaction on the $Co(OH)_2$/C catalyst is close to 3. This indicates that ORR occurs simultaneously via the 4- and 2-electron transfer pathways on the $Co(OH)_2$/C catalyst.

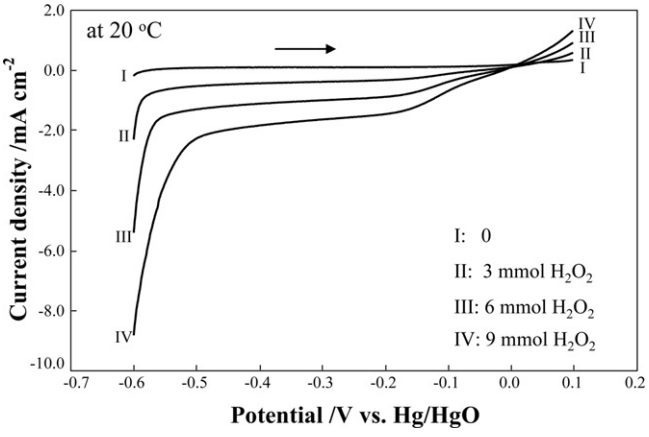

Fig. 9. Anodic potential–current relationship of $Co(OH)_2$/C modified glassy-carbon electrode in Ar-saturated NaOH solutions (1 M, pH 13.78) containing different contents of H_2O_2 at 20 °C. Scan rate: 10 mV s^{-1}. Catalyst loading: 2 mg cm^{-2}. Electrode area: 0.07 cm^2. Reference electrode: Hg/HgO/6 M KOH.

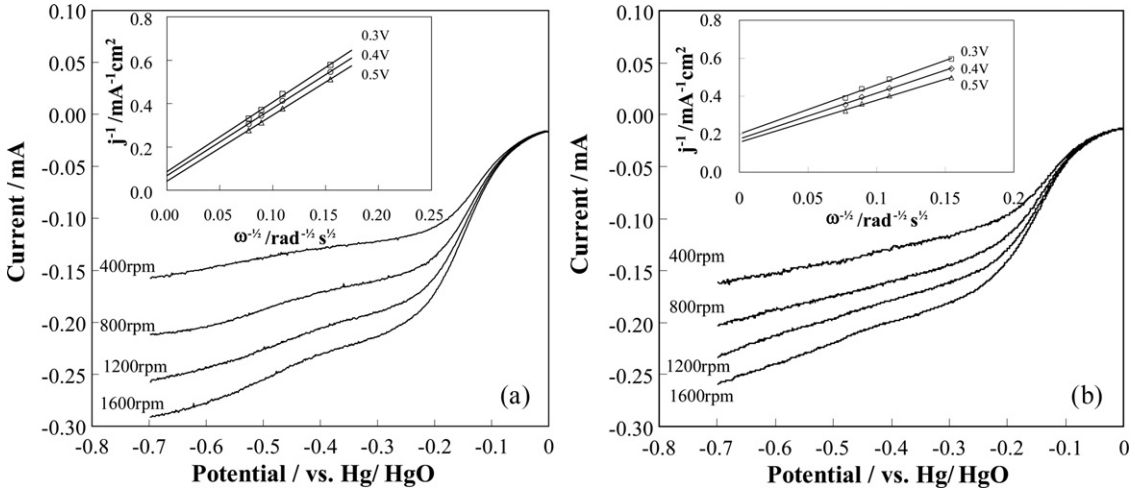

Fig. 10. RDE voltammograms obtained from (a) $Co(OH)_2$/C and (b) $Ni(OH)_2$/C electrodes in the O_2-saturated KOH solution (0.1 M, pH 12.93) at 25 °C. Scan rate: 10 mV s^{-1}. The inset shows Koutechy–Levich plots obtained at 0.3, 0.4, 0.5 V. Catalyst loading: 2 mg cm^{-2}. Electrode area: 0.07 cm^2. Reference electrode: Hg/HgO/6 M KOH.

Ramesh [23] studied CoOOH formation through various $Co(OH)_2$ oxidation methods. β-$Co(OH)_2$ has been proven to oxidize to β-CoOOH by dioxygen. $Co(OH)_2$ converts to CoOOH during ORR as shown in Fig. 4(a), and ORR occurs at the same potential as CoOOH reduction. Therefore, 4-electron ORR occurs on $Co(OH)_2$ through a sequential reaction process as follows:

(1) $Co(OH)_2$ reacts with O_2 to form CoOOH through the following reaction:

$$2Co(OH)_2 + ½O_2 = 2CoOOH + H_2O \quad (7)$$

(2) CoOOH converts to $Co(OH)_2$ through reaction (3) to complete the 4-electron ORR process:

$$2H_2O + O_2 + 4e^- = 4OH^- \quad (8)$$

In fact, reaction (8) is the stoichiometrical combination of reactions (3) and (7), indicating that the suggested 4-electron ORR route is reasonable.

3.2.2. ORR on $Ni(OH)_2$/C

The $Ni(OH)_2$/C-GC electrode exhibits a larger cathodic current peak area at 0.49 V when the electrode contains more $Ni(OH)_2$ as shown in the cyclic voltammograms in Fig. 6(b), indicating that NiOOH electroreduction reaction occurs at 0.49 V. The CVs of the $Ni(OH)_2$/C-GC electrode in the NaOH solutions saturated with Ar and O_2 are shown in Fig. 7(b). A cathodic peak current at −0.15 V appears, revealing that ORR on the $Ni(OH)_2$/C catalyst occurs at a lower potential than that on the $Co(OH)_2$/C catalyst. The small peak of ORR on $Ni(OH)_2$/C in the NaOH solution bubbled with O_2 for different time periods also indicates that the catalytic activity of the $Ni(OH)_2$/C catalyst is lower than that of the $Co(OH)_2$/C catalyst, as shown in Fig. 8(b). From the slopes of the K–L plots as shown in Fig. 10(b), the values of *n* for ORR on the $Ni(OH)_2$/C electrode are calculated to be 3.54, 3.79, 4.13 at 0.3, 0.4, and 0.5 V, respectively. The number of electrons exchanged in ORR on the $Ni(OH)_2$/C catalyst is assumed to be close to 4.

Fu et al. [24] examined the effect of oxidation temperature on nickel hydroxide formation. They found that NiOOH can be formed at a high temperature (60 °C) from β-$Ni(OH)_2$, but only a very small portion of the hydroxide was converted to oxyhydroxide at lower temperatures. The XRD results [in Fig. 4(b)] agree with those of Fu. More evidence can be found in the linear sweep voltammograms as shown in Fig. 8(b). If a considerable amount of NiOOH were formed during O_2 bubbling, a large cathodic current of NiOOH at the start potential of sweep (0 V) would have appeared. However, no distinct cathodic current was observed, revealing that $Ni(OH)_2$ was rather difficult to oxidize to NiOOH by dioxygen at 20 °C. Therefore, compared with the $Co(OH)_2$/C catalyst, the $Ni(OH)_2$/C catalyst has a lower content of oxyhydroxide (NiOOH) formed during ORR, which is considered to be one of the reasons for its poor catalytic activity toward ORR.

3.2.3. Temperature effect

Fig. 11 shows the cathode polarization behavior of $Co(OH)_2$/C or $Ni(OH)_2$/C in a DBFC at an alternating temperature of 60 and 20 °C. The operation temperature was regulated through supplying the fuel (alkaline borohydride solution) and humidified O_2 of different temperatures so that the cell operation temperature can be quickly shifted between 60 and 20 °C. The cathodes using $Co(OH)_2$/C and $Ni(OH)_2$/C exhibited similar polarization behavior at a high operation temperature (60 °C) but exhibited a distinct

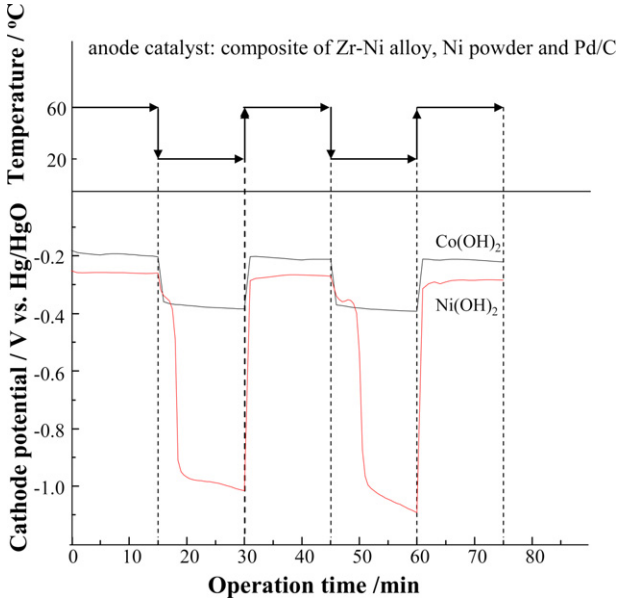

Fig. 11. A cathode potential comparison of the DBFC using $Ni(OH)_2$/C and $Co(OH)_2$/C as the cathode catalyst at alternating temperature of 60 °C and 20 °C. Anolyte: 5 wt.% of $NaBH_4$, 10 wt.% of NaOH, pH 14.19. Operation current density: 40 mA cm^{-2}. Catalyst loading: 10 mg cm^{-2}. Both anode and cathode area: 6 cm^2. Reference electrode: Hg/HgO/6 M KOH.

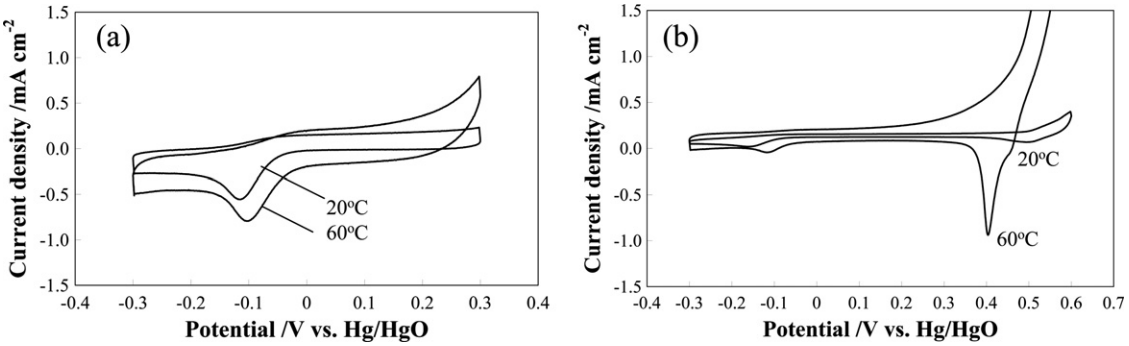

Fig. 12. Cyclic voltammograms of (a) $Co(OH)_2$/C and (b) $Ni(OH)_2$/C modified glassy-carbon electrodes at a scan rate of 10 mV s^{-1} in the Ar-saturated NaOH solution (1 M, pH 13.78) at 20 °C and 60 °C. Catalyst loading: 5 mg cm^{-2}. Electrode area: 0.07 cm^2. Reference electrode: Hg/HgO/6 M KOH.

polarization behavior at a low operation one (20 °C). The $Ni(OH)_2$/C cathode can only function within a short time period. However, the performance can be recovered and sustained at the same period at 20 °C after the cell was operated at 60 °C. This short stable performance is caused by the electroreduction of NiOOH formed when the cell is operated at 60 °C. The poor performance after the electroreduction of NiOOH to $Ni(OH)_2$ can be attributed to the poor electrocatalytic activity of $Ni(OH)_2$ toward ORR as mentioned in Section 3.2.2.

Notably, the operation potential of the $Ni(OH)_2$/C cathode is significantly improved after elevating the cell operation temperature to 60 °C as shown in Fig. 11. A simple temperature effect on the cathode performance improvement cannot explain this phenomenon because the $Co(OH)_2$/C cathode exhibits only a mild improvement in operation potential when the operation temperature is shifted from 20 to 60 °C.

Fig. 12 represents the cyclic voltammograms of the $Co(OH)_2$/C and $Ni(OH)_2$/C modified glassy-carbon electrodes in Ar-saturated NaOH solution at 20 and 60 °C. The redox reaction kinetics of the $Ni(OH)_2$/NiOOH couple is significantly improved by elevating the temperature as shown in Fig. 12(b). However, the $Co(OH)_2$/C electrode exhibits a mild improvement in redox reaction kinetics. The effect of temperature on the improvement of M(II)/M(III) redox reaction kinetics is coincident with that on the improvement of operation potential in the fuel cell as shown in Fig. 11. This result reveals that the redox reaction between NiOOH and $Ni(OH)_2$ plays an important role in ORR on the $Ni(OH)_2$/C catalyst.

Similar to the $Co(OH)_2$/C catalyst, the suggested ORR route in Section 3.2.1 is also suitable for the $Ni(OH)_2$/C catalyst. The 4-electron ORR occurs on $Ni(OH)_2$ through the chemical oxidation of $Ni(OH)_2$ to NiOOH:

$$2Ni(OH)_2 + \tfrac{1}{2}O_2 = 2NiOOH + H_2O \quad (9)$$

and then NiOOH is electrooxidized to $Ni(OH)_2$ based on reaction (4) during operation at a higher temperatures (say, 60 °C), so that $Ni(OH)_2$/C exhibits a higher operation potential. However, $Ni(OH)_2$ is difficult to oxidize to NiOOH at lower temperatures (say, 20 °C) according to the XRD results as shown in Fig. 4(b). Furthermore, the redox reaction of NiOOH to $Ni(OH)_2$ is retarded at lower temperatures. As a result, the $Ni(OH)_2$/C catalyst demonstrates poor electrocatalytic activity toward ORR at lower temperatures.

4. Model of ORR catalyzed by transition metal hydroxides

According to the experimental results and discussion on the ORR route on the $Co(OH)_2$/C and $Ni(OH)_2$/C catalysts, the ORR on transition metal hydroxides may occur simultaneously via the 2- and 4-electron transfer pathways. The 4-electron ORR process is related to the redox reaction of the hydroxyl group. Fig. 13 shows the XPS spectra of the $Co(OH)_2$/C and $Ni(OH)_2$/C catalysts. The top surface layer of these catalysts is composed of a hydroxide. This is understandable because ORR occurs at potentials lower than those of CoOOH and NiOOH electroreduction. Based on the XRD and XPS results as shown in Figs. 4 and 13, oxyhydroxide can be deduced to exist underneath the hydroxide layer of the catalyst. An ORR mechanism via the 4-electron transfer pathway on the carbon-supported hydroxide catalysts is summarized in Fig. 14. Oxyhydroxide (MOOH) accepts electrons through the carbon particles from the external circuit to convert to hydroxide. The hydroxide subsequently supplies electrons to the oxygen atom absorbed on the $M(OH)_2$ surface layer to form oxyhydroxide again. Meanwhile, OH^- ions are formed to complete the 4-electron ORR process.

Electroreduction reaction occurs with the use of metal hydroxide as a cathode catalyst in fuel cells. Otherwise, the fuel cell cannot

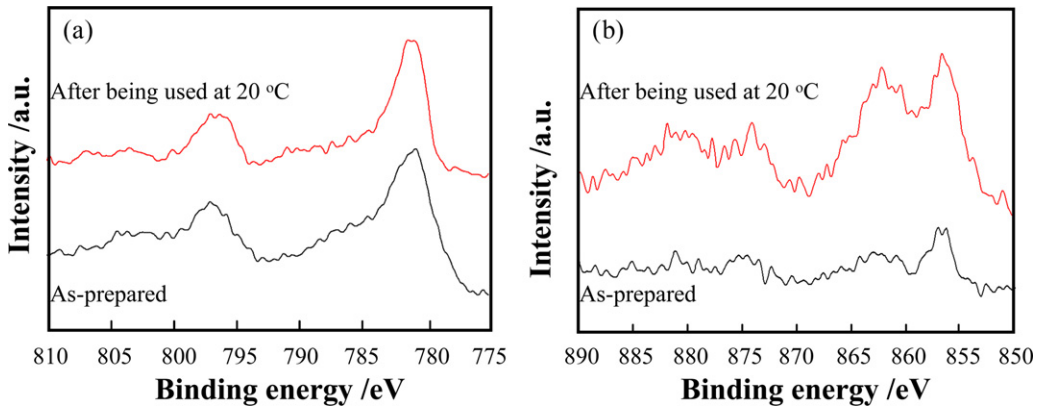

Fig. 13. Binding energies of (a) Co in the $Co(OH)_2$/C and (b) Ni in the $Ni(OH)_2$/C catalysts before and after use.

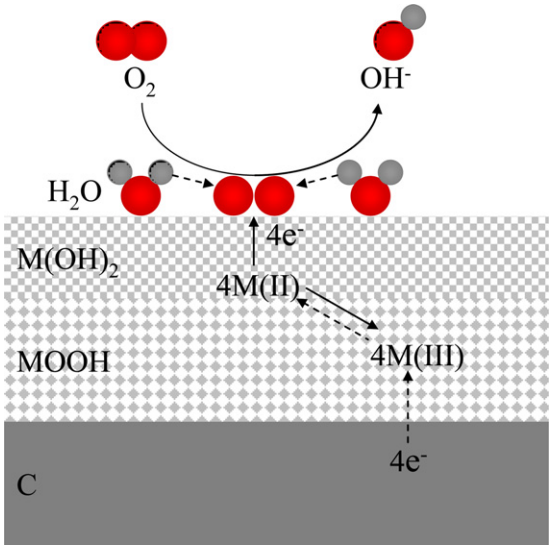

Fig. 14. Proposed redox cycle for the electrocatalytical reduction of oxygen to OH^- on hydroxide.

operate. Only the metal hydroxide at the cathode side can be oxidized by oxygen to form MOOH. This is due to oxygen being the only oxidant existing at the cathode side. As a result, MOOH electroreduction reaction occurs during fuel cell operation.

According to the suggested mechanism of ORR on hydroxides, the electrocatalytic activity of transition metal hydroxides toward ORR is considered to be dependent on the kinetics of the electroreduction of oxyhydroxide to hydroxide, and the oxidation kinetics of hydroxide by oxygen. Therefore, the improvement in electroreduction reaction kinetics of a redox couple and the oxidation kinetics of the compound with a lower chemical valence of the metal cation are key issues in the development of transition metal hydroxide catalysts with high electrocatalytic activity toward ORR.

5. Conclusions

ORR occurs via 4-electron reaction on the $Ni(OH)_2$/C catalyst, but it occurs simultaneously via the 4- and 2-electron transfer pathways on the $Co(OH)_2$/C catalyst. The ORR via the 4-electron transfer pathway on $Co(OH)_2$/C or $Ni(OH)_2$/C undergoes the following processes:

(1) oxidation of the hydroxide by O_2 to form the corresponding oxyhydroxide,
(2) electroreduction of the oxyhydroxide to regain the hydroxide.

$Co(OH)_2$ and $Ni(OH)_2$ have the same HCP structure and lattice parameters, but they exhibit different catalytic activities toward ORR at a low temperature. The poor catalytic activity of $Ni(OH)_2$/C at a lower temperature can be attributed to the difficulty of $Ni(OH)_2$ oxidation by O_2 and the slow kinetics of NiOOH electroreduction to $Ni(OH)_2$. The catalytic reactivity of the $Ni(OH)_2$/C catalyst can be significantly improved by elevating the operation temperature, due to the facts that NiOOH is easily formed, and the kinetics of NiOOH electroreduction reaction is improved during ORR.

Acknowledgements

This study was financially supported by the Hi-tech Research and Development Program of China (863), Grant No. 2007AA05Z144; the Doctoral Fund from Education Ministry of China (20070335003); China Postdoctoral Science Foundation (20090461364); and the National Natural Science Foundation of China, Grant Nos. 20976156 and 50971114.

References

[1] B. Wang, J. Power Sources 152 (2005) 1–15.
[2] Z.P. Li, B.H. Liu, J. Appl. Electrochem. 40 (2010) 475–483.
[3] S. Ohno, K. Yagyuu, K. Nakatsuji, F. Komori, Surf. Sci. 554 (2004) 183–192.
[4] B. Lescop, J.P. Jay, G. Fanjoux, Surf. Sci. 548 (2004) 83–94.
[5] H. Cheng, K. Scott, K. Lovell, Fuel Cells 6 (2006) 367–375.
[6] B.H. Liu, S. Suda, J. Power Sources 164 (2007) 100–104.
[7] K. Asazawa, K. Yamada, H. Tanaka, A. Oka, M. Taniguchi, T. Kobayashi, Angew. Chem. Int. Ed. 46 (2007) 8024–8027.
[8] R. Bashyam, P. Zelenay, Nature 443 (2006) 63–66.
[9] H.Y. Qin, Z.X. Liu, W.X. Yin, J.K. Zhu, Z.P. Li, J. Power Sources 185 (2008) 909–912.
[10] X.X. Yuan, X. Zeng, H.J. Zhang, Z.F. Ma, C.Y. Wang, J. Am. Chem. Soc. 132 (2010) 1754–1755.
[11] J.L. Fernández, D.A. Walsh, A.J. Bard, J. Am. Chem. Soc. 127 (2005) 357–365.
[12] Y. Liu, J.F. Ma, J.H. Lai, Y.N. Liu, J. Alloys Compd. 488 (2009) 204–207.
[13] H.Y. Qin, Z.X. Liu, S.J. Lao, J.K. Zhu, Z.P. Li, J. Power Sources 195 (2010) 3124–3129.
[14] H.Y. Qin, Z.X. Liu, L.Q. Ye, J.K. Zhu, Z.P. Li, J. Power Sources 192 (2009) 385–390.
[15] A.L. Bouwkamp-Wijnoltz, W. Visscher, J.A.R. van Veen, S.C. Tang, Electrochim. Acta 45 (1999) 379–386.
[16] F. Beck, J. Appl. Electrochem. 7 (1977) 239–245.
[17] J.H. Zagal, M.A. Paez, J.F. Silva, in: J.H. Zagal, F. Bedioui, J.P. Dodelet (Eds.), N_4-Macrocyclic Metal Complexes, Springer, New York, 2006, pp. 41–82.
[18] J.H. Zagal, M. Gulppi, M. Isaacs, G. Cardenas-Jiron, M.J.S. Aguirre, Electrochim. Acta 44 (1998) 1349–1357.
[19] J.R.T.J. Wass, I. Panas, J. Asbjornsson, E. Ahlberg, J. Electroanal. Chem. 599 (2007) 295–312.
[20] Z.P. Li, B.H. Liu, K. Arai, S. Suda, J. Electrochem. Soc. 150 (2003) A868–A872.
[21] V. Pralong, A. Delahaye-Vidal, B. Beaudoin, B. Gerand, J.-M. Tarascon, J. Mater. Chem. 9 (1999) 955–960.
[22] D. Zhang, D. Chi, T. Okajima, T. Ohsaka, Electrochim. Acta 52 (2007) 5400–5406.
[23] T.N. Ramesh, Ind. Eng. Chem. Res. 49 (2010) 1530–1533.
[24] X.Z. Fu, Y.J. Zhu, Q.C. Xu, J. Li, J.H. Pan, J.Q. Xu, J.D. Lin, D.W. Liao, Solid State Ionics 178 (2007) 987.